27 May 2010, 4:30 pm - 6:20 pm

Earthquake Induced Slope Failure Simulation by SPH

Ha H. Bui
Ritsumeikan University, Japan

R. Fukagawa
Ritsumeikan University, Japan

K. Sako
Ritsumeikan University, Japan

Y. Okamura
Ritsumeikan University, Japan


Fifth International Conference on
Recent Advances in Geotechnical Earthquake Engineering and Soil Dynamics
and Symposium in Honor of Professor I.M. Idriss
May 24-29, 2010 • San Diego, California

EARTHQUAKE INDUCED SLOPE FAILURE SIMULATION BY SPH

Ha H. BUI
Ritsumeikan University
Kusatsu, Shiga, 525-8577, Japan

R. FUKAGAWA, K. SAKO, Y. OKAMURA
Ritsumeikan University
Kusatsu, Shiga, 525-8577, Japan

ABSTRACT

Majority of slope stability, slope displacement and soil liquefaction analyses subjected to earthquake loading condition employed the finite element method (FEM) as the standard numerical tool. However, mechanism of soil failure in such condition often involved extremely large deformation and failure behaviors, which were unable to be modeled by FEM since this method was suffered from the grid distortion. In an attempt to overcome this limitation, we present herein our first attempt to extend the smoothed particle hydrodynamics (SPH) method to analyze slope failure behavior due to seismic shaking. For the sake of simplicity, effect of pore-water pressure was not taken into consideration. The numerical framework was then applied to simulate the failure behavior of a slope subjected to a seismic loading. Experimental model was also conducted to verify the numerical performance. It is shown that SPH can simulate fairly well the slope failure behavior in the model test, especially in prediction of the failure surface. The paper suggests that SPH should be considered as a powerful alternative for computation of geomaterials subjected to earthquake loading conditions.

INTRODUCTION

Computational applications of seismic slope stability analysis and earthquake induced slope failure simulation remain an active and important area of study in geotechnical engineering. In the last few decades, the seismic slope stability analysis has been often performed using the pseudo-static method and the sliding block method (Newmark, 1965). Although, these methods are simple and have some limitations, they are still widely used in the geotechnical applications.

On the other hand, in order to take into account the soil deformation behavior during earthquake, the finite element method (FEM) has been often applied. Advantage of FEM is that it took into account stress-strain relation of soil thus more accurate soil behavior can be taken into consideration. However, geotechnical problems subjected to earthquake loading condition often involved large deformation and failure of soil which were unable to be modeled using FEM due to the grid distortion problem. Re-meshed technique in FEM may help to resolve this problem but computational procedure is too complicated and it is quite difficult to apply to three dimensional problems. Therefore, there is a need to develop mesh-free methods for such computational purposes.

So far, the popular application of mesh-free method in geotechnical engineering is well known as the discrete element method (DEM), proposed by Cundall & Struck (1979). Advantages of this approach are that it can handle large deformation and failure problems, the concept is relatively simple and it is easy to implement computer code. However, DEM suffered from low accuracy since this method employed the interaction model, which was based on spring and dash-pot system whose parameters are difficult to determine. Another mesh-free method such as discontinuous deformation analysis (DDA) proposed by Shi et al. (1998) was also applied in geotechnical applications but mainly used for rock engineering, etc.

Alternatively, the smoothed particle hydrodynamics (SPH), proposed by Lucy (1977) and Gingold & Monaghan (1977), has been recently developed for solving large deformation and failure flows of geomaterials (Bui et al., 2007; 2008; 2009). The SPH method represents a powerful alternative for computational geomechanics especially for handling large deformation and post-failure of geomaterials, thereby providing physical insight to the failure mechanisms of soil.

In this paper, to enhance the application of SPH to computational geomechanics, the SPH method is extended to simulate the progressive failure of a slope subjected to an earthquake loading. Laboratory experiments were also conducted to verify the numerical result. In what follow, the numerical procedure and validation will be presented.

SIMULATION APPROACH

In this section, brief introduction about the simulation approaches will be explained.

SPH approximations

In the SPH method, a computational domain is modelled using a set of discrete particles, each is assigned with a constant mass and carries field variables at the corresponding location. The particles have a kernel function to define their interaction range, called the support domain, and the field variables are calculated through the use of an interpolation process over its neighboring particles located within the support domain. The interpolation process is based on the integral representation of a field function f(x) as follows,

$$\langle f(x)\rangle = \int_{\Omega} f(x')W(x-x',h)\,dx' \tag{1}$$

where x represents the location of particle; Ω specifies the influence domain of the integral; W is the basis function of the approximation, called the "kernel function"; h is the "smoothing length", which defines the influence domain of W; and this approximation $\langle\rangle$ is called "kernel approximation".

The kernel function W must be chosen to satisfy the following conditions:

$$\int_{\Omega} W(x-x',h)\,dx' = 1 \tag{2}$$

$$\lim_{h\to 0} W(x-x',h) = \delta(x-x') \tag{3}$$

where δ is the krecke detal function. Equation (2) ensures that a constant function of the space is exactly reproduced by equation (1), while equation (3) ensures a correct reproduction of the function when the smoothing length tends to zero.

The choice of kernel function directly affects the accuracy, efficiency and the stability of numerical algorithm. A number of kernel functions have been proposed in the SPH literature so far, we apply herein the most popular kernel function, namely cubic-spline function proposed by Monaghan and Gingold (1985), which has the following form,

$$W_{ij} = \alpha_d \times \begin{cases} \frac{2}{3} - q^2 + \frac{1}{2}q^3 & 0 \le q < 1 \\ \frac{1}{6}(2-q)^3 & 1 \le q < 2 \\ 0 & q \ge 2 \end{cases} \tag{4}$$

where α_d is the normalization factor which is $15/(7\pi h^2)$ in two-dimensional space and q is the normalized distance between particles i and j defined as $q = r/h$.

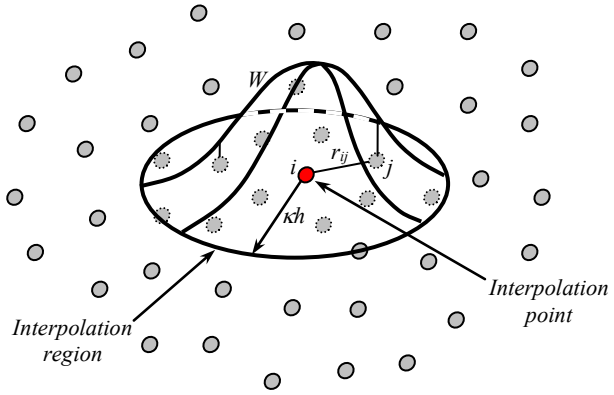

Fig. 1. SPH interpolation through particles.

The continuous integral representation (1) can now be discretized as a summation over the particles in the influence domain as follows,

$$\langle f(x)\rangle \approx \sum_{j=1}^{N} \frac{m_j}{\rho_j} f(x_j)W(x-x_j,h) \tag{5}$$

where j = 1, 2, …, N indicate particles within the influence domain of the particle at x, called neighboring; m_j and ρ_j are respectively the mass and the density of particle j. Fig.1 illustrates the approximation of this equation.

The approximation for the gradient $\nabla f(x)$ can be obtained simply by substituting $f(x)$ with $\nabla f(x)$ in equation (1). Integrating by parts and using the divergence theorem, one obtains

$$\langle \nabla f(x)\rangle \approx -\sum_{j=1}^{N} \frac{m_j}{\rho_j} f(x_j)\nabla W(x-x_j,h) \tag{6}$$

From equation (5) and equation (6), the particle approximation for a function and its gradient at a particle i can finally be written in condensed form as,

$$f(x_i) = \sum_{j=1}^{N} \frac{m_j}{\rho_j} f(x_j)W_{ij} \tag{7}$$

$$\nabla f(x_i) = \sum_{j=1}^{N} \frac{m_j}{\rho_j} f(x_j)\nabla W_{ij} \tag{8}$$

where

$$W_{ij} = W(x_i - x_j, h) \tag{9}$$

$$\nabla W_{ij} = \left(\frac{x_i - x_j}{r} \right) \frac{\partial W_{ij}}{\partial r} \quad (10)$$

with r is the relative distance between particles i and j. Further details of SPH integration scheme as well as other issues of SPH can be found in Liu and Liu (2004) or the SPH review of Monaghan (2005).

SPH discretization of motion equation

The motion equation of soil particles, in term of the effective stress, can be written in the following form,

$$\rho \ddot{u}^{\alpha} = \nabla_{\beta} \sigma'^{\alpha\beta} + \rho g^{\alpha} \quad (11)$$

where α and β denote Cartesian components x, y, z with the Einstein convention applied to repeated indices; ρ is the density; u is the displacement; σ' is the effective stress tensor, which is minus for compression; and g is acceleration due to the gravity.

Using equation (8), the partial differential form of equation (11) can be approximated in the SPH formulation in the following way,

$$\ddot{u}_i^{\alpha} = \sum_{j=1}^{N} m_j \left(\frac{\sigma_i'^{\alpha\beta}}{\rho_i^2} + \frac{\sigma_j'^{\alpha\beta}}{\rho_j^2} + C_{ij} \right) \nabla_{\beta} W_{ij} + g_i^{\alpha} \quad (12)$$

where C_{ij} is the stabilization term which was employed to remove the stress fluctuation and tensile instability found in SPH. The stabilization term C_{ij} consists of two components: artificial viscosity and artificial stress, which were computed similar to Bui et al. (2008) except that the sound speed, c, for the artificial viscosity term herein is calculated by,

$$c_i = \sqrt{\frac{E_i}{2\rho_i (1 + \upsilon_i)}} \quad (13)$$

where E is the Young's modulus of soil and υ is the Poisson's ratio.

Implementation of damping force to SPH

Motion of soil particles in SPH can be described using equation (12). However, under the seismic loading condition, this equation may not be enough to provide realistic soil performance since soil particles may have free vibration without damping. In order to obtain more realistic seismic behavior of soil particles in SPH, a damping force will be introduced into equation (12). In this paper, the non-viscous local damping force, proposed by Cundall (1987) for DEM, will be implemented into the SPH formulation. Accordingly, if the total force acing on particle i is denoted as $F_{(i)}$, the damping force acting on this particle will be calculated by,

$$F_{(i)}^{d} = \zeta \left| F_{(i)} \right| sign(v_i) \quad (14)$$

where

$$sign(v_i) = \begin{cases} +1, & \text{if} \quad v > 0; \\ -1, & \text{if} \quad v < 0; \\ 0, & \text{if} \quad v = 0 \end{cases} \quad (15)$$

The damping force is controlled by the non-dimensional damping constant ζ, whose value must be carefully chosen. In this paper, $\zeta = 0.2$ will be employed throughout our numerical test. Advantages of using this form of damping are that:

1. Only accelerating motion is damped. Therefore, no erroneous damping forces arise;
2. The damping constant is non-dimensional, thus it is easy to use; and
3. The damping is locally adaptive so that it varies from particle to particle and time to time.

The damping force will be added to the right hand side of equation (12) at every time step.

Soil constitutive model in SPH framework

Any soil constitutive models can be implemented into the SPH method using the framework proposed by Bui et al. (2007). In this paper, a simple elasto-plastic soil constitutive model in conjunction with the Drucker-Prager yield criterion is employed to model soil behavior. Details of discretization of this soil model in the SPH framework have been recently presented in Bui et al. (2008) we herein give brief description of this procedure to obtain the stress-strain relation.

A common approach to derive a stress-strain relation of soil is to use the classical plasticity. Accordingly, the total strain-rate tensor is often decomposed into two parts: an elastic strain rate tensor and a plastic strain rate tensor,

$$\dot{\varepsilon}^{\alpha\beta} = \dot{\varepsilon}_e^{\alpha\beta} + \dot{\varepsilon}_p^{\alpha\beta} \quad (14)$$

The elastic strain rate tensor can be calculated using the generalized Hooke's law, i.e.,

$$\dot{\varepsilon}_e^{\alpha\beta} = \frac{\dot{s}'^{\alpha\beta}}{2G} + \frac{1 - 2\upsilon}{E} \dot{\sigma}'^{m} \delta^{\alpha\beta} \quad (15)$$

where $s'^{\alpha\beta}$ is the deviatoric effective shear stress tensor; υ is Poisson's ratio; E is the elastic Young's modulus; G is the shear modulus and σ'^{m} is the mean effective stress.

The plastic strain rate tensor is calculated by the plastic flow rule, which is given by:

$$\dot{\varepsilon}_p^{\alpha\beta} = \dot{\lambda}\frac{\partial g_p}{\partial \sigma'^{\alpha\beta}} \tag{16}$$

where $\dot{\lambda}$ is the rate of change of plastic multiplier, and g_p is the plastic potential function. In the current study, the Drucker-Prager model with non-associated plastic flow rule is applied, under the assumptions that the yield surface is fixed in stress space, and plastic deformation occurs only if the stress state reaches the yield surface. Accordingly, plastic deformation will occur only if the following yield criterion is satisfied,

$$f(I_1, J_2) = \alpha_\phi I_1 + \sqrt{J_2} - k_c = 0 \tag{17}$$

where I_1 and J_2 are the first and second invariants of the stress tensor; and α_ϕ and k_c are Drucker-Prager constants that are calculated from the Coulomb material constants c (cohesion) and ϕ (internal friction). In plane strain, the Drucker-Prager constants are computed by,

$$\alpha_\phi = \frac{\tan\phi}{\sqrt{9 + 12\tan^2\phi}} \tag{18}$$

$$k_c = \frac{3c}{\sqrt{9 + 12\tan^2\phi}} \tag{19}$$

The *non*-associated plastic flow rule specifies the plastic potential function by,

$$g_p = \alpha_\psi I_1 + \sqrt{J_2} \tag{20}$$

where α_ψ relates to the dilatancy angle and it can be computed using equation (18) by replacing the friction angle (ϕ) with the dilatancy angle (ψ). Finally, substituting equation (20) into equation (16), and then equations (15-16) into equation (14), and additionally adopting the Jaumman stress rate for large deformation treatment, the final stress-strain relation for the current soil model at particle i becomes,

$$\begin{aligned}\frac{d\sigma_i'^{\alpha\beta}}{dt} &= \sigma_i'^{\alpha\gamma}\dot{\omega}_i^{\beta\gamma} + \sigma_i'^{\gamma\beta}\dot{\omega}_i^{\alpha\gamma} \\ &+ 2G_i\dot{e}_i^{\alpha\beta} + K_i\dot{\varepsilon}_i^{\gamma\gamma}\delta_i^{\alpha\beta} \\ &- \dot{\lambda}_i\left[3K_i\alpha_{\psi i}\,\delta^{\alpha\beta} + (G/\sqrt{J_2})_i s_i'^{\alpha\beta}\right]\end{aligned} \tag{21}$$

where $\dot{e}_i^{\alpha\beta} = \dot{\varepsilon}_i^{\alpha\beta} - \frac{1}{3}\dot{\varepsilon}_i^{\gamma\gamma}\delta^{\alpha\beta}$ is the deviatoric shear strain rate tensor; $\dot{\lambda}_i$ is the rate of change of plastic multiplier, which in SPH is specified by,

$$\dot{\lambda}_i = \frac{3\alpha_\phi K_i\dot{\varepsilon}_i^{\gamma\gamma} + (G/\sqrt{J_2})_i s_i'^{\alpha\beta}\dot{\varepsilon}_i^{\alpha\beta}}{9\alpha_\phi K_i\alpha_{\psi i} + G_i} \tag{22}$$

and $\dot{\varepsilon}_i^{\alpha\beta}$, $\dot{\omega}_i^{\alpha\beta}$ are the strain rate and spin rate tensors defined by

$$\dot{\varepsilon}_i^{\alpha\beta} = \frac{m_j}{2\rho_j}\left(\sum_{j=1}^{N}\dot{u}_{ji}^{\alpha}\nabla_\beta W_{ij} + \sum_{j=1}^{N}\dot{u}_{ji}^{\beta}\nabla_\alpha W_{ij}\right) \tag{23}$$

$$\dot{\omega}_i^{\alpha\beta} = \frac{m_j}{2\rho_j}\left(\sum_{j=1}^{N}\dot{u}_{ji}^{\alpha}\nabla_\beta W_{ij} - \sum_{j=1}^{N}\dot{u}_{ji}^{\beta}\nabla_\alpha W_{ij}\right) \tag{24}$$

The above soil constitutive model requires six soil parameters, which are the cohesion coefficient (c), friction angle (ϕ), dilatancy angle (ψ), and Young's modulus (E), Poission's ratio (υ), and soil density (ρ).

BOUNDARY CONDITIONS IN SPH

Boundary condition is one of the major issues in SPH that needs to be resolved. In this part, boundary conditions used to model solid boundary and earthquake loading will be explained.

Solid boundaries

In the SPH method, there have been several methods which were developed to model solid boundary conditions such as: ghost particles to model the free-slip boundary conditions (Libersky et al., 1993); repulsive force boundary condition (Monaghan, 1994; 1997; 2009); no-slip condition for viscous fluid (Takeda et al., 1994; Morris et al., 1997); stress boundary condition (Bui et al., 2008); etc. In this paper, we deal with two types of boundary conditions: free-roller and full-fixity. The free-roller boundary condition is modeled using ghost particles (Libersky et al., 1993), while the full-fixity one can be only modeled using the stress boundary method (Bui et al., 2008) whereby virtual particles are used to model the solid boundary and an additional procedure assigns velocity and stress to these boundary particles.

Earthquake loading

In order to model earthquake loading condition, seismic acceleration is applied directly to each SPH particle as the external load, rather than shaking from solid boundaries.

Accordingly, the SPH motion equation under earthquake is written as follows:

$$\ddot{u}_i^{\alpha} = \sum_{j=1}^{N} m_j \left(\frac{\sigma_i'^{\alpha\beta}}{\rho_i^2} + \frac{\sigma_j'^{\alpha\beta}}{\rho_j^2} + C_{ij} \right) \nabla_{\beta} W_{ij} + \bar{g}_i^{\alpha} \qquad (25)$$

where $\bar{g}$ is the modified gravitational acceleration due to earthquake defined by,

$$\bar{g}_i^{\alpha} = g_i^{\alpha} + a_{earthquake}^{\alpha} \qquad (26)$$

NUMERICAL PERFORMANCE AND VALIDATION

The proposed SPH method has been validated by comparison of the numerical result with data measured during suitable experiments. In these experiments, a small-scale cut slope model was subjected to seismic loading, generated by a vibration generation machine.

Experimental setup

Fig.2 shows the schematic diagram of the soil box and location of displacement sensors used for the slope model test. The soil box used in the model test is 100cm long, 60cm wide and 70cm high. The walls of the soil box are made of stainless plate, except the front side which is made of transparent reinforced glass in order to facilitate the observation of the slope failure process. Seven laser displacement sensors (ILD1300-200) were used to measure the displacement of the failure mass at some specific locations along the center of the slope model as shown in Fig.2. Three sensors, namely SH1-SH3, were affixed to right side of the soil box to measure the horizontal displacement of the failure mass, while four other

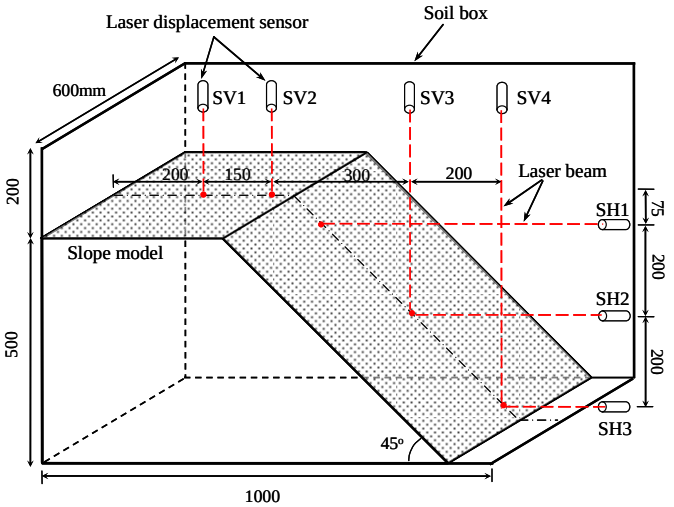

Fig. 2. Arrangement of slope mode test (unit in mm).

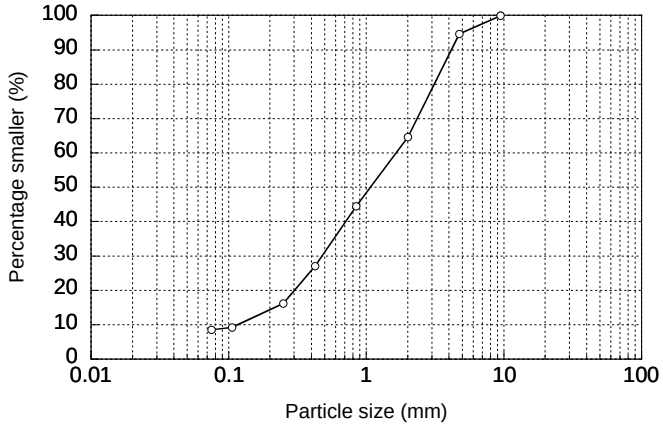

Fig. 3. Grain size distribution of Masa soil.

Table 1. Soil properties used for the slope model

Density (ρ)	Friction angle (ϕ)	Cohesion (c)	Young's modulus (E)	Poisson's ration (ν)
1.68	22.56°	0.78kPa	2.57MPa	0.33

Sensors, namely SV1-SV4, were located on the top of the soil box to measure the vertical displacement of the failure mass. The output signals from these sensors were sent to the analog output and finally to the computer.

The soil used in the current slope model experiment is Masa soil (weathered granite) which is the typical soil in Kansai region in Japan. The particle size distribution was measured by the laboratory test and the results are shown in Fig. 3. The maximum dry density was 1672kg/m^3 and the minimum one is 1297 kg/m^3.

Fig. 4. Overview of slope model after construction.

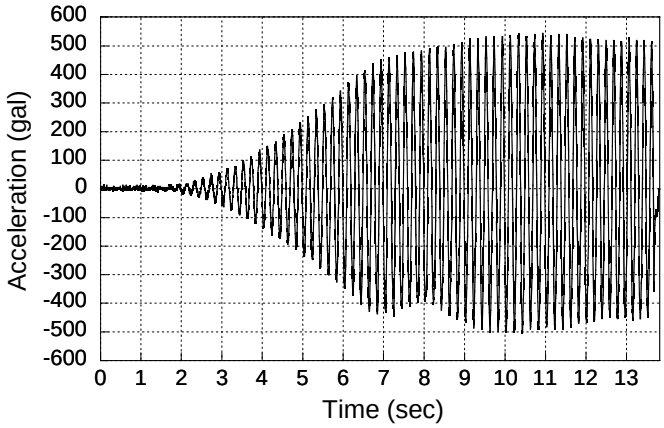

Fig. 5. Input earthquake wave in experiment

The slope model consisted of a homogenous soil slope which is 90cm long, 60cm wide, 50cm high, and inclined an angle of 45^o to the horizontal direction. The water content of soil was kept to approximate 10%. The shear strength parameters of the corresponding soil were measured from direct shear tests and the results are given in Table 1. The overview of the slope model after construction is shown in Fig.4.

The soil box model was placed on a vibration machine which can generate an earthquake with the maximum horizontal acceleration of 323m/s^2 and frequency of 700Hz. In this paper, the slope model was subjected to the horizontal shaking which has the wave form shown in Fig.4. The shaking was applied to the slope model until it was completely collapsed. It took about 12s to complete the experiment. The potential failure surface of the slope was then estimated by removing the failure soil.

Details of simulation

The 2D plane-strain simulation has been applied in the current simulation to reproduce the experiment. Soil is considered to be elastic-perfectly plastic material which can be modeled using the soil constitutive model presented foregoing. The soil parameters shown in Table 1 were employed in the current simulation and the dilatancy angle was assumed to be zero. The effect of pore-water pressure was therefore assumed negligible.

The slope shown in Fig.2 was modeled by 3275 SPH particles with an initial smoothing length of h = 1.20cm. Boundary conditions are free-roller at the left boundary, and full-fixity at the base. Similar to FEM, the initial stress condition within the slope must be obtained before applying the earthquake loading. In this paper, the initial stress was obtained by gradually applying the gravity to all particles. The initial configuration of the slope and corresponding vertical stress distribution is shown in Fig. 6.

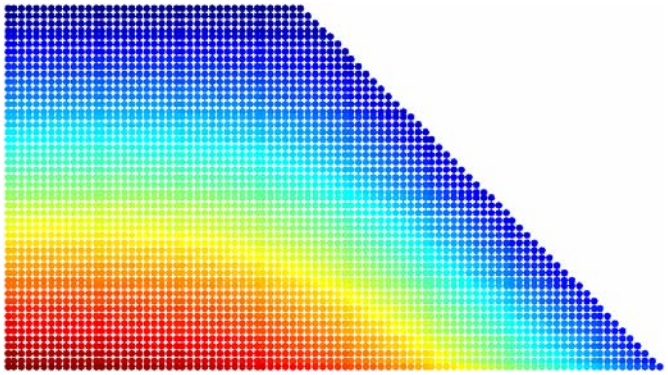

Fig. 6. Initial configuration and vertical stress distribution in the slope mode via SPH.

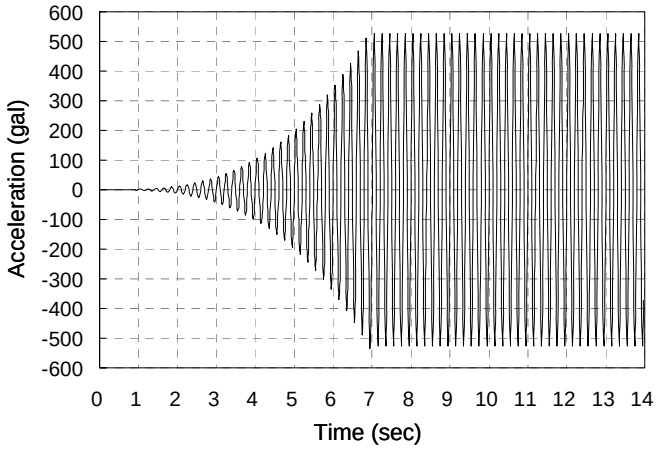

Fig. 7. Input earthquake wave in simulation

In order to reproduce the earthquake wave used in the experiment, an approximation sine wave function has been created and shown in Fig.7. This wave was then applied to the slope model through the horizontal of each particle using equation (25).

Discussion results

Fig.8 shows the comparison between the experiment and the SPH simulation for the final slope configuration at the end of earthquake loading. Four sliding surfaces and corresponding rotational blocks can be found from the experimental data, as shown in Fig. 8a. This suggests that the slope was collapsed in several stages during the earthquake. On the other hand, slope failure in the simulation occurred in one stage and only one rotational block can be simulated. Although, the SPH method can simulate well the post-failure process of the slope, it is quite difficult to reproduce exactly the failure mechanism obtained from experiment since the soil parameters in simulation were keep constant through out the numerical test.

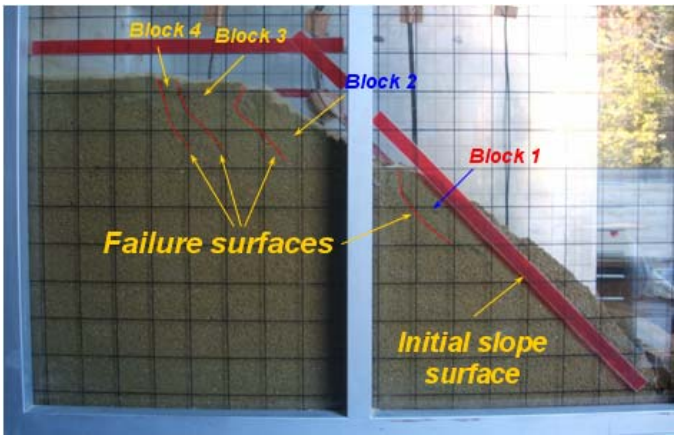

(a) Slope failure in experiment.

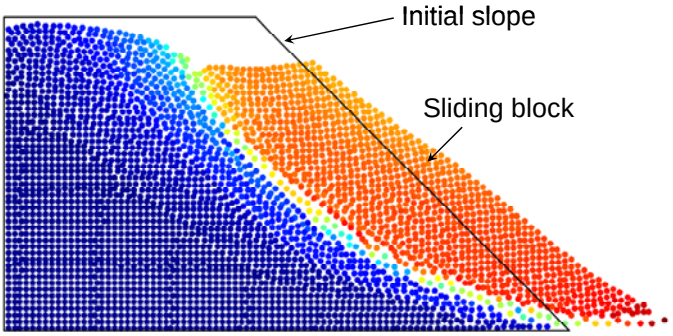

(b) Slope failure in simulation.

Fig. 8. Slope configurations at the end of the earthquake loading obtained from the experiment and the SPH simulation.

It would be better to implement a more advanced soil model that accounts for the change of soil parameters during the earthquake shaking. Such works are postponed to our future work.

Fig. 9 shows the comparison of the failure surface between experiment and simulation. It is interesting to notice that the numerical simulation result agrees fairly well with the failure surface of the last failure mode in the experiment. The shape of failure surface in the simulation is almost circular, while that of experiment seems to be straight line. It is not clear about this failure mechanism since there may have some technical errors when removing the failure soil to specify the failure surface in our experiments. Further tests will be conducted to clarify this difference.

Regarding the displacement of the sliding mass at the center of the slope, Fig.10 and Fig.11 show the comparison between experiment and simulation for the horizontal and vertical displacements of the sliding mass. It can see that the simulation results can qualitatively predict the tendency developments of the horizontal and vertical displacements of

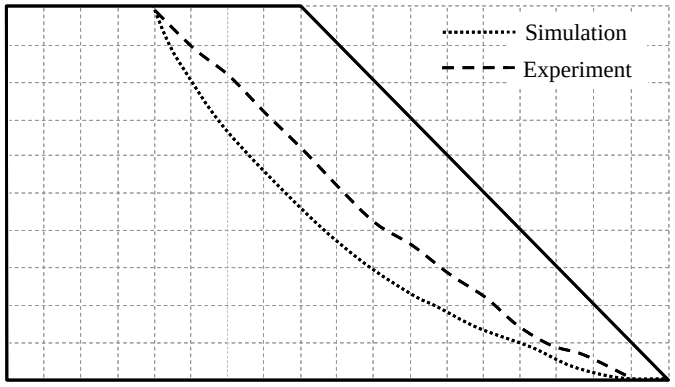

Fig. 9. The observed slip surface of the last sliding block as compared to the slip surface predicted by SPH.

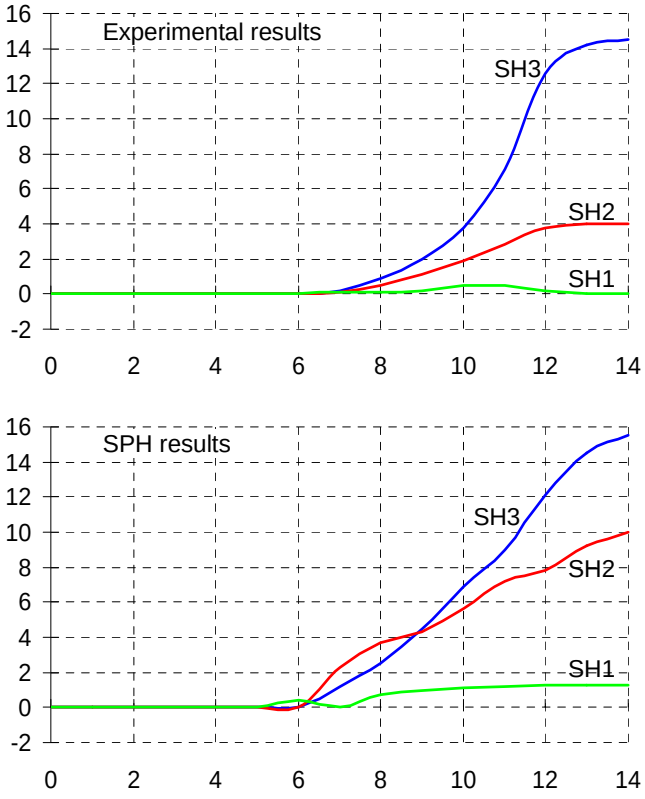

Fig. 10. Comparison of failure horizontal displacement between the experiment and the SPH simulation.

the failure mass. However, the simulations results overestimated the experimental data. Furthermore, the slope failure in the simulation started at about 1s earlier than that in experiment. It seems that the proposed damping force hasn't been satisfied yet for the current SPH application. Further studies are needed to investigate these differences. On the other hand, the current numerical results confirmed the advantage of SPH which is over the traditional method in handling post-failure behavior of soil during earthquake.

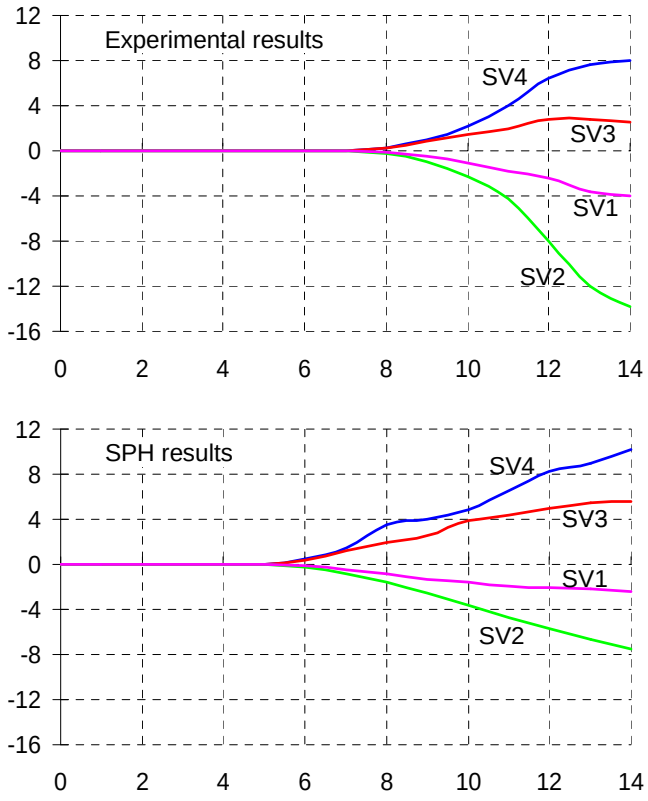

Fig. 11. Comparison of failure vertical displacement between the experiment and the SPH simulation.

CONCLUSION

The SPH method in conjunction with an elasto-plastic (Drucker-Prager) stress-strain model has been shown to be a reliable and robust method for post-failure behavior simulation of a slope subject to earthquake loading. Numerical simulation can predict fairly well the experiment data, although some results are overestimated. The authors are encouraged by these results but recognize the need for further improvement of the numerical method. Advantage of the method is its robustness, conceptual simplicity, relative ease of incorporating new physics, and especially its potential to handle large deformation and post-failure behaviors.

REFERENCES

Cundall, P.A., O.D.L. Strack [1979]. "A discrete numerical model for granular assemblies". Géotechnique 29, 47-65.

Cundall, P.A. [1987] "Distinct element methods of rock and soil structures". In: E.T. Brawn, Editor, Analytical and computational methods in engineering rock mechanics, Allen.

Bui, H.H. [2007]. "Lagrangian mesh-free particle method (SPH) for large deformation and post-failure of geomaterials using elasto-plastic soil constitutive models". Ritsumeikan University, Japan, Ph.D. thesis.

Bui, H.H., K. Sako, R. Fukagawa [2007]. "Numerical simulation of soil-water interaction using smoothed particle hydrodynamics (SPH) method". J. Terramech. 44, No. 5, 339-346.

Bui, H.H., R. Fukagawa, K. Sako., S. Ohno [2008]. "Lagrangian mesh-free particle method (SPH) for large deformation and post-failure of geomaterial using elastic-plastic soil constitutive model". Int. J. Numer. Anal. Methods Geomech. 32, No. 12, 1537-1573.

Bui, H.H., K. Sako, R. Fukagawa. [2009]. "Slope stability analysis and slope failure simulation by SPH". 17th Int. Conf. for. Soil Mech. Geotech. Eng. (ICSSMGE), No. 2, 1578-1581.

Bui, H.H., R. Fukagawa, K. Sako. [2009]. "Slope stability analysis and runout prediction of slope failure by SPH". Proc. Int. Sym. Geo-informatics and Zoning for Hazard Map., 174-177.

Gingold, R.A., J.J. Monaghan [1977]. "Smoothed particle hydrodynamics: Theory and application to non spherical stars". Mon. Not. Roy. Astron. Soc., 181, 375-389.

Liu, G.R., M.B. Liu [2004]. "Smoothed Particle Hydrodynamics: A Mesh-free Particle Method". World Scientific.

Lucy L. [1977]. "A numerical approach to testing the fission hypothesis". Astrono. J. 82, 1013-1024.

Monaghan, J.J., J.C. Lattanzio [1985]. "A refined particle method for astrophysical problems". A. & A. 149: 135-143.

Monaghan, J.J. (1994). "Simulating Free Surface Flows with SPH". J. Comput. Phys. 110, 399-406.

Monaghan, J.J. [2005]. "Smoothed particle hydrodynamics". Rep. Prog. Phys. 68, No. 8, 1703-1759.

Morris, J.P., P.J. Fox, Y. Zhu [1997]. "Modeling low Reynolds number flows using SPH". J. Comput. Phys. 136, 214-226.

Libersky, L.D., A.G. Petschek, T.C. Carney [1993]. "High Strain Lagrangian Hydrodynamics: A 3D SPH code for dynamic material response". J. Comput. Phys. 109, 67-75.

Shi, G.H. [1988]. "Discontinuous deformation analysis: a new numerical model for the static and dynamics of block systems". University of California, USA, Ph.D. thesis.

Takeda, H., S.M. Miyama, M. Sekiya [1994]. “Numerical simulation of viscous flow by smoothed particle hydrodynamics”. Prog. Theor. Phys. 92, No. 5, 939-960.